# A dimensionless study of the evaporation and drying stages in spray pyrolysis

N. Reuge, B. Caussat *

*Laboratoire de Génie Chimique/ENSIACET/INPT, UMR CNRS 5503, 5 rue Paulin Talabot, BP1301, 31106 Toulouse Cédex 1, France*

**Abstract**

An original dimensionless study of the pure evaporation and precipitation stages of a spray pyrolysis process has been performed. An estimation of the evaporation time is proposed and the influence of the main processing parameters has been investigated. For operating conditions corresponding to industrial requirements, the main limiting step of the evaporation stage is thermal transfer from the column walls to the gas, not mass or thermal transfer at the droplet surface. Therefore, gas and liquid temperatures remain equal and constitutive equations can be greatly simplified. Moreover, in these conditions, neither solute concentration nor temperature gradients exist inside micronic droplets. Some data from the literature have been modelled and show the large range of validity of the equations and explanations proposed. Finally, with the assumptions made here, the dimensionless study of the precipitation stage shows that the presence of a crust can increase the drying time four-fold. However, a filled particle can still be formed.

*Keywords:* Spray pyrolysis; Drying; Modelling; Dimensionless study; Precipitation; Hollow particles

## 1. Introduction

Spray pyrolysis (SP) is an aerosol process commonly used to produce a wide variety of materials in powder form (Gurav, Kodas, Pluym, & Xiong, 1993; Pratsinis & Vemury, 1996) including metals, metal oxides, ceramics, superconductors, fullerenes and nanostructured materials. The technology has been used for many years in the materials, chemicals and food industries. It consists in five main steps: (i) generation of a spray from a liquid precursor by an appropriate droplet generator, (ii) spray transport by air flow during which solvent evaporation occurs then concomitant solute precipitation when the solubility limit is exceeded in the droplets, (iii) thermolysis of the precipitated particles at higher temperatures to form micro/nanoporous particles, (iv) intra-particle sintering to form dense particles, (v) finally, extraction of the particles from the gas flow. SP offers specific advantages over conventional material processing techniques (Gurav et al., 1993; Pratsinis & Vemury, 1996) (gas-to-particle conversion processes, liquid or solid-state processing followed by milling), such as a higher purity of the powders produced, a more uniform chemical composition, a narrower size distribution, a better regularity in shape and the synthesis of multi-component materials. Another advantage is the relative simplicity of the process, which allows easy scale-up (Joffin, 2004).

However, challenges still exist for SP, e.g. to increase production rates, to better understand the influence of the operating conditions or to control particle size, shape and internal morphology, ... Three main types of particle morphology can be obtained: (i) completely filled or "solid" nanoporous particles, (ii) microporous particles and (iii) hollow (shell-like) particles. For instance, Lyons, Ortega, Wang, and Kodas (1992) obtained hollow MgO and ZnO particles and full $Al_2O_3$ particles from nitrate salt precursors. No change in particle size or morphology was observed in nitrate-derived ZnO or MgO by modifying the initial air humidity or the heating rate. The addition of small amounts of seed particles with or without (i) an initially saturated drying environment and (ii) temperature gradient modifications in the flow system also had no effect. However, Lengorro, Hata, and Iskandar (2000) observed a radical change in the morphology of $ZrO_2$ particles with a diameter of about 3 μm, from hollow

* Corresponding author. Tel.: +33 5 34615211; fax: +33 5 34615253.
*E-mail addresses:* reuge@free.fr (N. Reuge), Brigitte.Caussat@ensiacet.fr (B. Caussat).

**Nomenclature**

| | |
|---|---|
| $a_w$ | water activity |
| $Cp$ | specific heat (J kg$^{-1}$ K$^{-1}$) |
| $c_s$ | solute concentration in droplet (mol m$^{-3}$) |
| $c_{s,0}$ | solute concentration in the initial solution (mol m$^{-3}$) |
| $c_s^{css}$ | critical super saturation concentration of the solute (mol m$^{-3}$) |
| $\Delta c/c$ | defined by relation (21) |
| $D_{cr}$ | diffusivity of vapour through the crust (m$^2$ s$^{-1}$) |
| $D_v$ | binary diffusion coefficient of air/water vapour (m$^2$ s$^{-1}$) |
| $D_{w,s}$ | binary diffusion coefficient of solute/liquid water (m$^2$ s$^{-1}$) |
| $D_v^p$ | apparent diffusion coefficient of water vapour through the crust (m$^2$ s$^{-1}$) |
| $F$ | mass flow rate (kg s$^{-1}$) |
| $h_{vap}$ | vapourization enthalpy of water (J kg$^{-1}$) |
| $H$ | total distance required for the evaporation stage (m) |
| $K$ | constant defined by relation (15) (m$^2$ s$^{-1}$) |
| $M$ | molar weight (kg mol$^{-1}$) |
| $P_{sat}$ | saturation pressure of water vapour in air (Pa) |
| $P_1$, $P_2$ | dimensionless numbers defined by relations (7) |
| $P_3$ | dimensionless number defined by relation (20) |
| $P_4$ | dimensionless number defined by relation (26) |
| $P_5$ | dimensionless number defined by relation (33) |
| $q$ | heat flux density transferred from the column wall to the spray (W m$^{-2}$) |
| $q^*$ | dimensionless heat flux defined by relation (6) |
| $r$ | distance along droplet/particle radius (m) |
| $r_{int}$ | position of air/liquid interface along droplet/particle radius (m) |
| $R$ | droplet radius (m) |
| $R_c$ | column radius (m) |
| $R_p$ | droplet radius at the onset of precipitation (m) |
| $R^*$ | relative droplet radius (m) |
| $R_p^{0D}$ | droplet radius at the onset of a volume precipitation (m) |
| $s^*$ | parameter defined by relation (33) |
| $t$ | time (s) |
| $t_{evap}$ | total time of evaporation (s) |
| $t_{drying}$ | total time of particle drying (s) |
| $t_v$ | characteristic time of diffusion of water vapour in air (s) |
| $t_{w,s}$ | characteristic time of diffusion of solute/water (s) |
| $T$ | temperature (K) |
| $T^*$ | relative temperature defined by relation (6) |
| $v_z$ | mean gas velocity along reactor axis (m s$^{-1}$) |
| $w_a$, $w_w^{vap}$ | mass fractions of air/water vapour in gas |
| $w_s^{liq}$ | mass fraction of solute in droplet |
| $w_w^{liq}$ | mass fraction of liquid water in droplet |
| $X$, $Y$ | relative mass fractions defined by relation (1) |
| $Y_{int}$ | defined by relation (A.5) |
| $\Delta Y$ | defined by relation (3) |
| $z$ | axial coordinate (m) |
| $z^*$ | relative axial distance defined by relation (6) |

*Greek symbols*

| | |
|---|---|
| $\alpha$ | thermal diffusivity (m$^2$ s$^{-1}$) |
| $\beta_c$ | parameter defined by relation (18) |
| $\varepsilon$ | porosity of the crust |
| $\lambda$ | thermal conductivity (W m$^{-1}$ K$^{-1}$) |
| $\rho$ | density (kg m$^{-3}$) |
| $\tilde{\rho}$ | mean density (kg m$^{-3}$) |
| $\tau$ | tortuosity of the crust |
| $\chi$ | parameter defined by relation (33) |

*Subscripts*

| | |
|---|---|
| a | air |
| d | droplet |
| gas | gas |
| liq | liquid |
| p | precipitate |
| s | solute |
| w | water |
| 0 | initial value |

to completely filled spheres, by changing the process temperature.

Concerning the evaporation stage, some characteristic dimensionless numbers have already been used by Lyons et al. (1992), Xiong and Kodas (1993) and Sano and Keey (1982) to briefly introduce or interpret their modelling results. A more detailed dimensionless description has been performed by Jayanthi, Zhang, and Messing (1993), but only regarding their own processing conditions. It appears that ratios of characteristic times of water vapour diffusion in air, of solute diffusion in water or of thermal diffusion in the solution and the total evaporation time are key dimensionless parameters to understand the phenomena occurring in the gas and in the liquid phases. But most of these dimensionless investigations only consider individual droplets and not the global behaviour of a spray.

Moreover, the precipitation/evaporation stage, also called the drying stage (Messing, Zhang, & Jayanthi, 1993), has not been really seriously studied, excepted by Nesic and Vodnik (1991): from experiments and numerical investigations, they succeeded in finding a good model to describe the diffusion of evaporating water through the particle crust.

In the present work, in a first part an exhaustive dimensionless study of the evaporation stage was carried out in a general way. The aim was to determine the influence of each operating parameter on the process and the main limiting steps for a wide range of processing conditions. We first assume uniform solute concentrations inside the droplets and estimate in particular the evaporation time, the difference between water vapour partial pressures in air and at the droplet surface and the difference between gas and liquid temperatures as a function of processing conditions.

Then, we studied mass and thermal transfers inside droplets to determine the conditions for which concentration and temperature gradients do or do not exist inside droplets in SP. The dimensionless equations developed were then applied to data from the literature to demonstrate their large range of validity and also to discuss the mechanisms responsible for the results obtained by various authors.

In a last part, the precipitation/evaporation stage (or drying stage) was investigated: the influence of the operating parameters on the particle morphology and of the structural parameters of the crust (i.e. porosity and tortuosity) on the drying time was analysed.

## 2. Dimensionless study of the pure evaporation stage

### *2.1. 1D dimensionless model assuming uniform solute concentration inside droplets*

#### *2.1.1. Assumptions and equations*

A 1D model at the scale of the column and a 0D model at the scale of the droplet were developed first. It was of practical interest to use the following dimensionless expressions:

$$X = w_w^{liq} w_s^{liq^{-1}}, \qquad Y = w_w^{vap} w_a^{-1} \tag{1}$$

where $w_a$ and $w_w^{vap}$ are the mass fractions of air/water vapour in the gas, $w_w^{liq}$ the mass fraction of liquid water in a droplet, and $w_s^{liq}$ is the mass fraction of the solute in the droplet.

The equation of mass conservation of water is therefore given by

$$F_a Y + F_s X = F_w \tag{2}$$

where air, water and solute flow rates $F_a$, $F_w$ and $F_s$ are expressed in kg/s.

Then, the following assumptions were made:

(i) gas flow is laminar,
(ii) all parameters are uniform in droplets (0D),
(iii) at the reactor scale, momentum, heat and mass transfer phenomena in the radial direction can be ignored (1D), as assumed by (Jayanthi et al., 1993; Lengorro et al., 2000; Xiong & Kodas, 1993; Yu & Liao, 1998),
(iv) axial conductive heat transport in the spray and axial diffusion of water vapour in air can be neglected over convective phenomena,
(v) pure air is considered for the thermal properties of the gas phase,
(vi) pure water is considered for the thermal properties and for the density of the solution,
(vii) gas/spray velocity is constant along the reactor,
(viii) the relative velocity between droplets and carrier gas is zero and there is no interaction between droplets,
(ix) the Kelvin effect is negligible (i.e. droplets remain much larger than 0.1 μm (Hinds, 1982)),
(x) the water activity $a_w$ in the solution remains equal to 1,
(xi) the specific humidity of air is equal to zero at the reactor inlet,
(xii) the heat flux density $q$ transferred from the column wall to the spray is constant along the reactor,
(xiii) all water is evaporated during this stage (i.e. no solubility limit is considered), and
(xiv) $F_s$ is much smaller than $F_w$.

In this approach, four equations must be solved: the mass conservation at the reactor scale (2) and at the droplet scale (3), the energy equation at the reactor scale (4) and at the droplet scale (5). With the aforementioned assumptions, the dimensional expressions of the last three are given in Appendix A.1. In a dimensionless form, they can be written as

$$\Delta Y = Y_{int} \frac{T^*_{gas}}{T^*_{liq}} - Y = \rho_w (3\rho_a)^{-1} P_2 P_1^{-2/3} (P_1 - Y)^{-1/3} \frac{\partial Y}{\partial z^*} \tag{3}$$

$$Cp_w Cp_a^{-1} P_1 \frac{\partial T^*_{liq}}{\partial z^*} + \frac{\partial T^*_{gas}}{\partial z^*} + h_{vap} (Cp_a T_0)^{-1} \frac{\partial Y}{\partial z^*} = q^* \tag{4}$$

$$T^*_{gas} - T^*_{liq} = \rho_w Cp_w D_v (3\lambda_a)^{-1} P_2 (1 - P_1^{-1} Y)^{2/3} \frac{\partial T^*_{liq}}{\partial z^*} + \rho_a h_{vap} D_v (\lambda_a T_0)^{-1} \Delta Y \tag{5}$$

$Y_{int}$ is the reduced water mass fraction at the droplet/gas interface at saturation pressure, depending on $T_{liq}$ as detailed in Appendix A.1. Three dimensionless variables and two dimensionless numbers have been used:

$$z^* = z H^{-1}, \qquad T^* = T T_0^{-1}, \qquad q^* = 2\pi R_c H q (F_a Cp_a T_0)^{-1} \tag{6}$$

$$P_1 = (F_w + F_s) F_a^{-1} \quad \text{and} \quad P_2 = t_v t_{evap}^{-1} \tag{7}$$

$P_1$ is a mass dilution ratio and $P_2$ is a ratio of two characteristic times (Lyons et al., 1992), i.e., the characteristic time of water vapour diffusion in air $t_v$ (Jayanthi et al., 1993) and the total time of pure evaporation of the spray in the drying column $t_{evap}$, which are given by

$$t_v = R_0^2 D_v^{-1} \quad \text{and} \quad t_{evap} = H v_z^{-1} \tag{8}$$

As demonstrated in Appendix A.1, the dimensionless radius $R^*$ can be written as

$$R^* = R R_0^{-1} = (1 - P_1^{-1} Y)^{1/3} \tag{9}$$

Thus, the whole 1D + 0D problem depends on two dimensionless numbers ($P_1$ and $P_2$). Of course, the dimensionless flux $q^*$ must be adjusted in such a way that the stage of pure evaporation is complete at $z^* = 1$. Actually, this stage ends at the onset of precipitation. Taking the supersaturation limit into account would introduce additional parameters specific to the salts that would prevent the feasibility of a general dimensionless study. This is why assumptions (xiii) and (xiv) have been made. Thus, the evaporation stage is assumed to be complete when all the water has been evaporated, i.e., when

$$Y = F_w F_a^{-1} \approx P_1 \tag{10}$$

Or in other words, when $R^* = 0$. This is not a severe limitation of the study since its results could be easily corrected taking the onset of precipitation as the end of this stage.

The dimensionless equations were implemented in the finite element solver FlexPDE (FlexPDE 5, 2006), which uses a modified Newton–Raphson iteration process, an automatic mesh generator with dynamic adaptative refinement. This latter function is essential when numerous calculations have to be performed over a wide range of processing conditions such as in this study. Note that the code has been numerically validated implementing the same equations in the most conventional ODE solver Scilab which uses an Euler scheme.

Calculations were performed for a wide range of values of $P_1$ and $P_2$, initial values of $T_{liq}$ and $T_{gas}$ being fixed at 20 °C. In all, 54 different operating conditions were tested.

### 2.1.2. Results and discussion

All the results obtained will be commented as a function of $P_1$ and $P_2$. So, it is obvious that such a study will be useful to experimentalists only if it is possible to determine the values of the two dimensionless numbers from given processing parameters. Unfortunately, the determination of $P_2$ cannot *a priori* be known because the knowledge of the total time of the evaporation stage $t_{evap}$ requires complete resolution of the problem. However, an analytical expression of $t_{evap}$ can be deduced from the results of the dimensionless study for the whole range of processing conditions studied as detailed below.

The calculated values of $q^*$ versus $P_1$ and $P_2$ are presented in Fig. 1. From these results, the following relation can be deduced:

$$q^* = 10P_1 + 9200P_2 \tag{11}$$

For values of the ratio $P_2/P_1$ lower than $10^{-4}$, the calculated values of $q^*$ depend only on $P_1$ and are equal to about $10P_1$. Small values of $P_2/P_1$ correspond to small droplet diameters, low heating rates and/or dense sprays. This means that for these conditions, the total flux needed for complete evaporation of droplets is proportional to the mass dilution ratio. From this result and from relations (6) and (8), the following relation can be obtained as detailed in Appendix A.1:

$$t^{\dagger}_{evap_1} = 5(\rho_a C p_a T_0) R_c P_1 q^{-1} = 1.6 \times 10^6 R_c P_1 q^{-1} \tag{12}$$

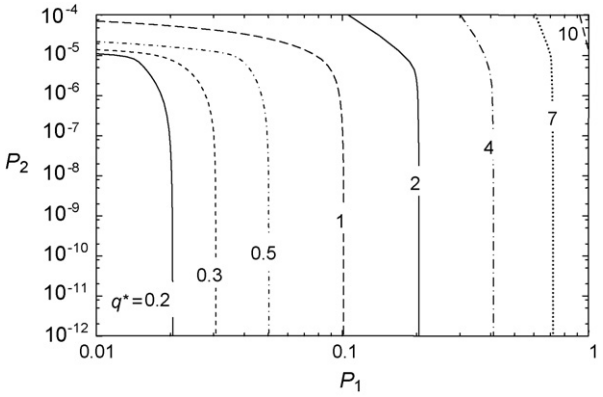


Fig. 1. Values of the dimensionless flux $q^*$ calculated vs. $P_1$ and $P_2$.

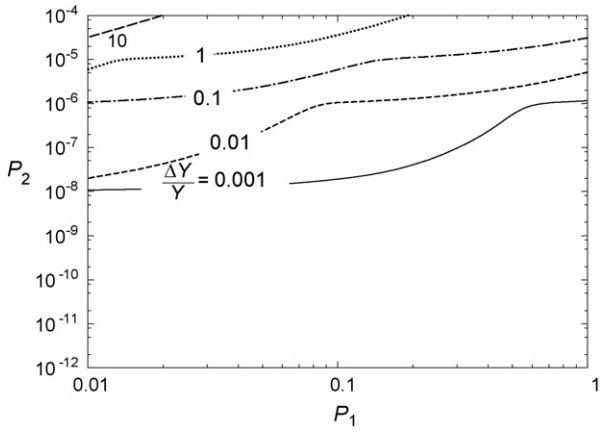


Fig. 2. Mean values of $\Delta Y/Y$ calculated vs. $P_1$ and $P_2$.

Relation (12) shows that the total time of evaporation is proportional to the reactor diameter and to the mass dilution ratio and inversely proportional to the heat flux density.

On the other hand, for values of $P_2/P_1$ greater than $10^{-4}$, $q^*$ (and therefore also $t_{evap}$) varies with both $P_1$ and $P_2$. From (6), (8) and (11), the following relation can be obtained as detailed in Appendix A.1:

$$t_{evap_1} = \frac{t^{\dagger}_{evap_1}}{2} + \sqrt{\left(\frac{t^{\dagger}_{evap_1}}{2}\right)^2 + 4600(\rho_a C p_a T_0) R_0^2 R_c D_v^{-1} q^{-1}}$$
$$= \frac{t^{\dagger}_{evap_1}}{2} + \sqrt{\left(\frac{t^{\dagger}_{evap_1}}{2}\right)^2 + 1.49 \times 10^9 R_0^2 R_c D_v^{-1} q^{-1}} \tag{13}$$

Thus, when $P_2/P_1$ is greater than $10^{-4}$, the total time of evaporation also varies with the droplet diameter. Note that if $P_2/P_1$ was greater than $10^{-2}$ (conditions at the limit of the range of this study, corresponding to the evaporation of an isolated droplet rather than to a spray), the dimensionless flux and the evaporation time would not depend on $P_1$ anymore.

Then, mean values of the ratio $\Delta Y/Y$ along the column axis were calculated versus $P_1$ and $P_2$ as reported in Fig. 2. This relative difference varies mainly with $P_2$, and is negligible for $P_2$ lower than $10^{-6}$. For these latter operating conditions, currently encountered in SP and corresponding to small droplet diameters and low heating rates, the limiting step of the evaporation process is thermal transfer from the column walls to the spray and not mass transfer at the air/water interface. Therefore, the water vapour pressure at the droplet surface is always very close to the interfacial saturation pressure and the reduced mass fraction of water vapour in air $Y$ is almost equal to $Y_{int}(T_{gas}/T_{liq})$. Hence, in these conditions, relation (9) and equations of energy (4) and (5) are sufficient to model the evaporation stage.

Fig. 3 presents the difference between gas and liquid temperatures averaged along the column axis. As we can see, as long as $P_2$ is lower than $10^{-6}$, gas and liquid temperatures are almost

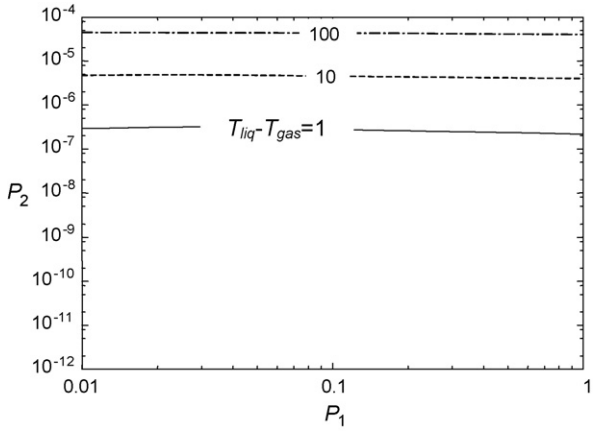


Fig. 3. Mean difference of gas/liquid temperature calculated vs. $P_1$ and $P_2$.

equal. This means that the limiting step of the evaporation process is thermal transfer from the reactor walls to the gas and not thermal transfer at the air/water interface. Hence, the first equation of energy (4) is sufficient to solve the evaporation problem and the droplet radius can be written as

$$R^* = (1 - P_1^{-1} Y_{\text{int}})^{1/3} \tag{14}$$

Since $Y_{\text{int}}$ is a function of liquid temperature, the dimensionless droplet radius depends only on the local temperature and not on the thermal history of the spray.

Then, analysing the temporal evolutions of $R^*$ calculated by our dimensionless study, we noticed that the so-called $D^2$-law (i.e. linear plot of droplet area versus residence time) was a relatively good approximation for the evaporation process whatever the values of $P_1$ and $P_2$. This law, experimentally determined by Schlünder (1964) and Ranz and Marshall (1952) and validated by modelling studies using the conventional equations of evaporation spray (Yu, 1995; Yu & Liao, 1998), can be written as

$$R^2 = R_0^2 - Kt \tag{15}$$

where $K$ is a constant.

Note that all these results and tendencies do not depend on assumptions (xiii) and (xiv), excepted relations (12) and (13). However as detailed below, it is now possible to give an estimation $t_{\text{evap}_2}$ of the total time of evaporation taking the onset of precipitation as the end of this stage.

At the onset of precipitation, the droplet radius takes the following expression:

$$R_{\text{p}}^{0\text{D}} = R_0 \left( \frac{c_{\text{s},0}}{c_{\text{s}}^{\text{css}}} \right)^{1/3} \tag{16}$$

where $c_{\text{s}}^{\text{css}}$ is the critical supersaturation concentration of the solute. Then, from (15) we can write

$$\frac{R_0^2}{t_{\text{evap}_1}} = \frac{R_0^2 - R_{\text{p}}^{0\text{D}^2}}{t_{\text{evap}_2}} \tag{17}$$

And from (16) and (17), we have

$$t_{\text{evap}_2} = \beta_{\text{c}} t_{\text{evap}_1} \quad \text{with } \beta_{\text{c}} = 1 - \left( \frac{c_{\text{s},0}}{c_{\text{s}}^{\text{css}}} \right)^{2/3} \tag{18}$$

where $t_{\text{evap}_1}$ is given by relations (12) or (13). Thus, the aforementioned tendencies deduced from relation (13) are still valid for (18). Additionally, this latter relation shows that the closer the initial solute concentration is to the critical supersaturation concentration, the shorter the total time of evaporation.

As an example of numerical application, an experimental and modelling study of $Y(NO_3)_3$/water droplet evaporation was carried out in our group. For the following parameters: $P_1 = 0.1$, $R_{\text{c}} = 0.1$ m, $q = 390$ W/m$^2$ and $\beta_{\text{c}} = 0.9$, the total time of evaporation calculated elsewhere by a precise model was of 35 s (Reuge et al., 2006). It has been estimated at 34 s using relation (18).

Thus, relation (18) provides a good estimation of the total time of pure evaporation. Note that several methods exist to determine the heat flux density $q$. It is not usually constant along the reactor, but its mean value can be considered.

### 2.2. 1D model at the droplet scale

#### 2.2.1. Assumptions and equations

Knowing that the previously mentioned parameter $K$ remains constant during the drying step and assuming that mass transport in the droplet is purely diffusive, it can be mathematically shown that the solute concentration inside the droplet takes the following form in steady-state conditions (Gardner, 1964):

$$c_{\text{s}}(r) = c_{\text{s}}(0) \exp[P_3 r^2 R^{-2}] \tag{19}$$

with

$$P_3 = \tfrac{1}{4} K D_{\text{w,s}}^{-1} \tag{20}$$

Thus, the relative solute concentration between the centre and the interface of the droplet can be written as

$$\frac{\Delta c}{c} = \frac{c_{\text{s}}(R) - c_{\text{s}}(0)}{c_{\text{s}}(0)} = \exp(P_3) - 1 \tag{21}$$

As long as the relative concentration $\Delta c/c$ between the centre and the interface of a droplet is lower than about 0.2, a first order Taylor expansion of its expression (21) can be performed, and as a result $\Delta c/c$ is equal to $P_3$.

Then, from (10) and (16), we obtain the following estimation for $K$:

$$K = \frac{R_0^2 - R_{\text{p}}^{0\text{D}^2}}{t_{\text{evap}}} = \frac{R_0^2}{t_{\text{evap}}} \beta_{\text{c}} \tag{22}$$

And therefore, the dimensionless number $P_3$ is given by

$$P_3 = \tfrac{1}{4} \beta_{\text{c}} t_{\text{w,s}} t_{\text{evap}}^{-1} \quad \text{with } t_{\text{w,s}} = R_0^2 D_{\text{w,s}}^{-1} \tag{23}$$

In this expression, logically, the characteristic time of solute diffusion in water $t_{\text{w,s}}$ and the total time of evaporation $t_{\text{evap}}$ both appear.

By using relations (14), (18) and (23), an estimation of the relative solute concentration only dependent on operating

parameters can finally be obtained:

$$\frac{\Delta c}{c} = P_3 = \frac{1}{4} R_0^2 D_{w,s}^{-1} \left[ 8 \times 10^5 R_c P_1 q^{-1} + \sqrt{\left(8 \times 10^5 R_c P_1 q^{-1}\right)^2 + 1.49 \times 10^9 R_0^2 R_c D_v^{-1} q^{-1}} \right]^{-1} \quad (24)$$

*2.2.2. Results*

As long as $P_3$ is lower than about $10^{-2}$, concentration gradients inside droplets can be considered as negligible. From relation (23), this condition is favoured by long times of evaporation and small droplet radii. Note that for salts, the binary diffusion coefficient of solute/liquid water $D_{w,s}$ is always in the range $10^{-9}$ to $2 \times 10^{-9}$ m$^2$ s$^{-1}$ (Reid, Prausnitz, & Sherwood, 1977) and varies little whatever the processing conditions.

From relation (24), the formation of large solute concentration gradients is promoted by rapid heating, large initial radii of droplets and low dense sprays (i.e. small values of $P_1$). The smaller the value of $P_2/P_1$, the greater the dependence on the two latter parameters (i.e. $R_0$ and $P_1$). All these tendencies agree with numerous modelling studies found in the literature (Jayanthi et al., 1993; Reuge et al., 2006; Xiong & Kodas, 1993; Yu & Liao, 1998).

If non-negligible solute concentration gradients exist inside droplets, the critical supersaturation is obviously reached first at the droplet surface. Thus, the droplet radius $R_p$ at the onset of precipitation is greater than $R_p^{0D}$ and can be determined from relations (16) and (19) as detailed in Appendix A.2:

$$R_p = R_p^{0D} \left[ \frac{2}{3} \left( P_3^{-1} - \frac{\sqrt{\pi}}{2 P_3^{3/2}} \frac{\mathrm{erfi}(\sqrt{P_3})}{e^{P_3}} \right)^{-1} \right]^{1/3} \quad (25)$$

For values of $P_3$ lower than 1, the effect of the formation of solute concentration gradients inside a droplet on its final radius is not significant: it is less than 10% greater than that obtained with a uniform solute concentration. Most size analysis techniques are not sufficiently accurate to detect such small differences, as mentioned by Jayanthi et al. in their modelling study of drying of ZHC/water droplets (Jayanthi et al., 1993). Values of $P_3$ greater than 1 are not usually encountered in SP.

In a manner similar to solute/water diffusion in the droplet, the heat brought by the reactor walls and then by the carrier gas diffuses from the droplet surface to its centre. Thus, it can be shown that the relative temperature gradients inside droplets can be estimated by the following dimensionless number (Hinds, 1982; Xiong & Kodas, 1993):

$$P_4 = \beta_c (R_0^2 \alpha_d^{-1}) t_{evap}^{-1} \quad (26)$$

where $\alpha_d$ is the droplet thermal diffusivity. In this expression the ratio of the characteristic time of thermal diffusion in the solution ($R_0^2/\alpha_d$) logically appears as does the total time of evaporation $t_{evap}$. Note that $P_4$ is different from the classical thermal Biot number which is sometimes inadequately used to justify this assumption. The ratio of $P_4$ and of $P_3$ is equal to $\alpha_d D_{w,s}$ and its value is usually very small (typical values for $D_{w,s}$ and $\alpha_d$ are of about $10^{-9}$ and $10^{-7}$ m$^2$ s$^{-1}$, respectively, in aqueous solutions). Thus, the number $P_4$ is usually lower than $P_3$ by several orders of magnitude. The assumption of uniform temperature in droplets is therefore always true in SP, except in very unusual conditions in which the heating is extremely rapid.

*2.2.3. Discussion of the results found in the literature*

In our previous study of micronic $Y(NO_3)_3$/water droplet evaporation (Reuge et al., 2006), $P_3$ was about $2 \times 10^{-5}$ (using (24)). Xiong and Kodas (1993) worked on the evaporation process of a spray of micronic NaCl/water droplets; $P_3$ was about $2.5 \times 10^{-6}$. Therefore, no gradient can appear for these specific conditions, nor in a wide range of conditions around them. These results were confirmed in these two studies by models and calculations based on exact descriptions of mass transfer inside droplets.

Different values of $\Delta c/c$ calculated at the onset of precipitation reported in the literature are presented in Fig. 4 versus $P_3$ (calculated with (22)) and in Table 1: for Yu and Liao (1998) (millimetric $NH_4NO_3$/water droplets) and for Jayanthi et al. (1993) (ZHC/water droplets, $R_0 = 10$ μm), the agreement is good between the calculated values of $\Delta c/c$ and the values of $P_3$. The value of $\Delta c/c$ calculated by Sano and Keey (1982) (millimetric skimmilk/water droplets) is large and greatly overestimated by relation (22) (the reasons behind this discrepancy will be explained later). Typically, the initial droplet radii of these latter studies (Sano & Keey, 1982; Yu & Liao, 1998) were larger

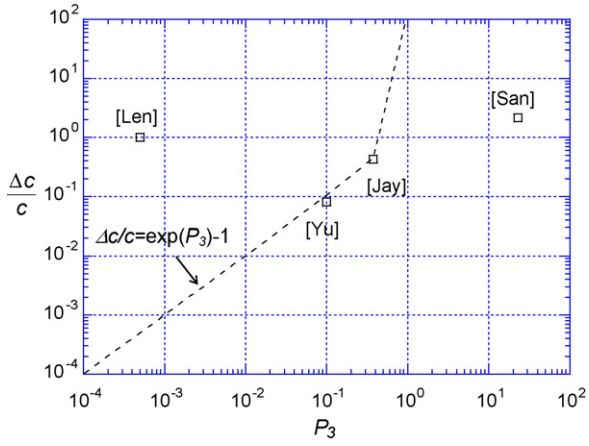


Fig. 4. Values of $\Delta c/c$ calculated vs. $P_3$ from literature data.

Table 1
Values of $P_3$ and $\Delta c/c$ obtained by the different authors cited in the text

| Reference | $P_3$ | $\Delta c/c$ |
|---|---|---|
| Xiong and Kodas (1993) | $2.5 \times 10^{-6}$ | Insignificant |
| Reuge et al. (2006) | $2 \times 10^{-5}$ | Insignificant[a] |
| Lengorro et al. (2000) | $5 \times 10^{-4}$ | 1.0 |
| Yu and Liao (1998) | 0.1 | 0.08 |
| Jayanthi et al. (1993) | 0.38 | 0.43 |
| Sano and Keey (1982) | 23.0 | 2.16 |

[a] Lower than accuracy of calculations.

than the initial droplet radii in the former studies. In the case of Jayanthi et al. (1993), solute concentration gradients exist inside droplets despite their micronic size because an extremely intense heating rate is assumed in the simulation.

Lengorro et al. (2000) worked on micronic ZHC/water droplet evaporation and calculated very strong solute concentration gradients at the onset of precipitation ($\Delta c/c \approx 1$). As can be seen in Fig. 4, such a value of $\Delta c/c$ is obtained with a $P_3$ of about 0.4. However, their operating conditions lead to a value of $P_3$ of about $5 \times 10^{-4}$: no solute concentration gradient can *a priori* appear. The reason for this disagreement has not been identified.

Then, consider cases for which significant solute concentration gradients logically appear. It must be noted that for given operating parameters, the dimensionless number $P_3$ is constant and does not depend on the degree of evaporation (or evaporation time). As a consequence, with the considered assumptions, $\Delta c/c$ in the droplet should be constant all along the reactor. In fact, since the concentration profile is uniform just after droplet generation, at the onset of evaporation, there is first a short transient stage during which $\Delta c/c$ increases, and then a steady state of diffusion during which it is constant. Let us consider calculated values of $\Delta c/c$ in the literature and let us try to estimate the duration of the transient stage. In the case of Yu and Liao (1998), all the calculated values of $\Delta c/c$ are very close to 0.08 (see Fig. 5 in Yu & Liao, 1998), and therefore the first reported concentration profile (at $t = 32$ s) belongs to the stationary stage. In the case of Jayanthi et al. (1993), all calculated values of $\Delta c/c$ are very close to 0.45 (see Fig. 1 in Jayanthi et al., 1993), and therefore the first reported concentration profile (at $t = 0.05$ s) already belongs to the stationary stage. On the other hand, in the case of Sano and Keey (1982), $\Delta c/c$ is always increasing (see Fig. 7a in Sano & Keey, 1982): here, the stationary stage is not reached even after a time of 52.7 s. This is a particular case where the solute (skimmilk) is not a salt and where the diffusion coefficient $D_{w,s}$ (of about $10^{-11}$ to $10^{-10}$ m$^2$/s) is much lower than the previous ones (of about $10^{-9}$ m$^2$/s). This explains the length of the transient stage and the discrepancy between the calculated value of $\Delta c/c$ and $P_3$. Note that the duration of the transient stage can be very roughly estimated by the value of $t_{w,s}$ (relation (23)); this time is equal to 100, 0.1 and $10^4$ s for (Yu & Liao, 1998), (Jayanthi et al., 1993) and (Sano & Keey, 1982), respectively.

From these results, the existence of a critical initial concentration can be deduced. Indeed, if the initial concentration is lower than a critical value, the stationary stage is reached before the onset of precipitation, and the final solute concentration gradient is the same whatever the initial concentration. If the initial concentration is greater than this critical value, the onset of precipitation occurs during the transient stage, and the final solute concentration gradient is dependent on the initial concentration. The results reported by Jayanthi et al. (1993) in their Fig. 3 can now be explained: for initial concentrations of 0.5 and 4 mol/l, the calculated final solute concentration gradient is almost the same ($\Delta c/c$ of about 0.86). However, for their initial concentration of 5.7 mol/l, very close to the solubility limit, the calculated final solute concentration gradient is lower ($\Delta c/c$ of about 0.39). Therefore, in this case the critical initial concentration is between 4 and 5.7 mol/l.

Finally, it appears that ultrasonic nebulisers are often used as droplet generators for SP because they allow high production rates well suited to industrial requirements (Joffin, 2004; Messing et al., 1993; Reuge et al., 2006; Xiong & Kodas, 1993). Such generators produce relatively dense aerosols of micronic droplets typically requiring several tens of seconds to be evaporated (Messing et al., 1993). Our dimensionless study shows that the evaporation stage of micronic or sub-micronic droplets with such conventional conditions does not involve the formation of solute concentration gradients. However, these typical times can be reduced by several orders of magnitude if the air flux used for spray generation is preheated. For instance, in the experimental and modelling study performed by Shabde et al. (2005), which deals with the drying of 10–80 μm droplets to produce hollow micropolymeric particles, the heating of droplets by preheated air is so rapid that the model considers that evaporation only begins to occur once the boiling point of the solvent is reached. And of course, strong solute concentration gradients appear.

In conventional conditions, as mentioned above, it can be concluded that modification of any of the operating parameters controlling the evaporation stage has no impact on the final morphology of the particles (provided $P_3$ remains small). Regarding the global optimisation of SP, this result can be quite useful.

Moreover, reduction of coalescence phenomena is another key issue of the process. It can be done, without loss of production capacity by increasing the heating rate and/or the air flow rate, or using a moderately preheated air flux to decrease the evaporation time (after precipitation, coalescence does not occur anymore). Nevertheless, note that the increase of the air flow rate is limited since the gas flow must remain laminar: turbulence would promote additional coalescence phenomena.

## 3. Dimensionless study of the precipitation stage and considerations about the formation of hollow particles

### 3.1. Modelling of the precipitation stage

Once the solute reaches the critical supersaturation concentration somewhere in the droplet, the solution begins to precipitate.

If the solute concentration is uniform at this time, volume precipitation occurs and usually particle of varying density is quickly formed. In the case of homogeneous nucleation and assuming that the droplet/particle radius remains equal to $R_p^{0D}$, the porosity of the formed particle is given by

$$\varepsilon = 1 - \frac{M_s c_s^{css}}{\rho_p} \tag{27}$$

where $M_s$ is the molar weight of the solute and $\rho_p$ is the density of the precipitate (the physical density, not the bulk density).

But as reported by Jayanthi et al. (1993) on the basis of the work of Zallen (1983) on percolation threshold, the volume fraction filled by the precipitate in a particle of radius $R_p$ must exceed a critical value to obtain a coherent porous network. This latter

is of about 0.16, i.e., a formed "solid" particle cannot exceed a critical porosity of 0.84. In the case of a uniform solute concentration at the onset of precipitation, this constraint is usually satisfied.

If a solute concentration gradient exists at the onset of precipitation, as previously said, the solution begins to precipitate at the droplet surface where the solute concentration has reached the critical supersaturation. Then, two cases must be considered (Jayanthi et al., 1993):

- *Case 1*. The solute concentration at the particle centre is greater than or equal to the equilibrium saturation concentration.

  In this case, the precipitation front moves quickly from the particle surface to its centre. As previously, volume precipitation occurs and a solid particle is obtained provided the volume fraction of the precipitate exceeds 0.16. The local porosity of the particle formed is now a function of the radial position and is given by

$$\varepsilon(r) = 1 - \frac{M_s c_s(r)}{\rho_p} \tag{28}$$

  where $c_s(r)$ is the solute concentration at the radial position $r$ at the onset of precipitation. Therefore, the porosity increases toward the particle centre.

  If the volume fraction of the precipitate exceeds 0.16 toward the particle surface but not toward the particle centre, a hollow particle is obtained.
- *Case 2*. The solute concentration at the particle centre is lower than the equilibrium saturation concentration.

  In this case, the precipitation front moves quickly from the particle surface to the radial position for which the solute concentration is equal to saturation (still considering the volume fraction of the precipitate exceeds 0.16). Toward the particle centre, the solute concentration is too low to allow precipitation and the phase remains liquid. Therefore, at this moment, the particle formed is hollow. The porosity of the crust is also given by relation (28).

But what occurs then during the next stages of the SP process? Authors usually conclude that the fate of the particle is irremediably to stay hollow. However, as long as the crust formed is porous (which is necessarily the case if nucleation is homogeneous), water can continue to evaporate at the liquid/air interface inside the pores and the inner liquid phase continues to precipitate progressively. Eq. (A.1) is still valid to describe the process of evaporation ($X$ is now non-uniform, its value at the liquid/air interface must be now considered and $R$ must be taken as equal to $R_p$) considering the following modified diffusion coefficient of air/water vapour:

$$D_v^p = D_v \left(1 + \frac{D_v}{D_{cr}} \frac{R_p - r_{int}}{r_{int}}\right)^{-1} \tag{29}$$

where $D_{cr}$ is the diffusivity of vapour through the precipitated layer and $r_{int}$ is the radial position of the liquid/air interface. This latter expression of an apparent diffusion coefficient $D_v^p$ was experimentally determined by Nesic and Vodnik (1991). The diffusivity $D_{cr}$ can be expressed as a function of the crust porosity $\varepsilon$ and tortuosity $\tau$:

$$D_{cr} = \frac{\varepsilon}{\tau} D_v \tag{30}$$

Porosity varies between $r_{int}$ and $R_p$, but for calculations we will consider its value at the crust surface where it is the smallest.

Then, Eq. (A.1) can be written as (see Appendix A.3):

$$\tilde{\rho}_{liq} \left(\frac{dr_{int}^2}{dt}\right)_{crust} = -2 \frac{R_p}{r_{int}} D_v^p \rho_a \Delta Y \tag{31}$$

By considering now the same droplet of radius $r_{int}$ but without a crust, Eq. (A.3) becomes

$$\tilde{\rho}_{liq} \left(\frac{dr_{int}^2}{dt}\right)_{no\ crust} = -2 D_v \rho_a \Delta Y \tag{32}$$

Then, using $P_5 = \varepsilon/\tau$ and $s^* = r_{int}^2/R_p^2$, we have

$$\chi = \frac{(ds^*/dt)_{crust}}{(ds^*/dt)_{no\ crust}} = \left(\sqrt{s^*}(1 - P_5^{-1}) + P_5^{-1}\right)^{-1} \tag{33}$$

Knowing that the evolution of $s^*$ would be linear with time if there was no crust, we can perform an integration of $1/\chi$ to know the ratio of the drying time of the remaining water with crust and of the drying time of remaining water without crust:

$$\frac{t_{drying}^{crust}}{t_{drying}^{no\ crust}} = \frac{1}{s_0^*} \int_0^{s_0^*} \chi^{-1}\, ds^* = P_5^{-1} + \frac{2}{3}(1 - P_5^{-1})\sqrt{s_0^*} \tag{34}$$

with $s_0^* = r_{int,0}^2/R_p^2$, where $r_{int,0}$ is the radial position of the liquid/air interface just after the onset of precipitation.

Note that $t_{drying}^{no\ crust}$ can be easily determined from the value of $t_{evap}$ and from the $D^2$-law, and then, $t_{drying}^{crust}$ can also be determined from relation (34).

### 3.2. Results

Calculated values of $\chi$ have been reported in Fig. 5 as a function of $P_5$ and $s^*$. The dashed areas correspond to domains in which relation (33) no longer has any physical signification:

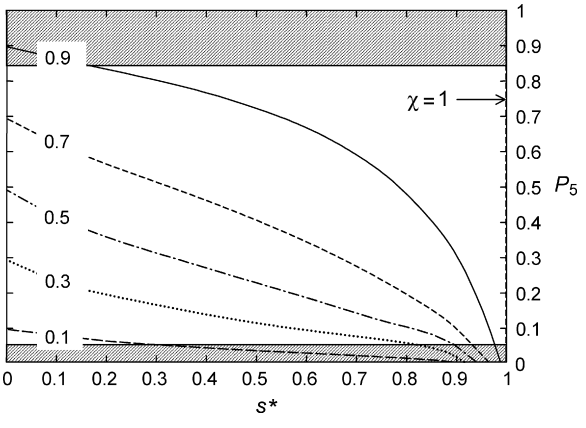


Fig. 5. Values of $\chi$ calculated vs. $P_5$ and $s^*$.

as mentioned earlier, a coherent porous medium cannot have a porosity greater than 0.84, and moreover, a percolation threshold exists (Hilfer, 1996) below which the pores are no longer connected (the critical porosity has been arbitrarily fixed at 0.05 in Fig. 5).

It appears that $\chi$ decreases when $P_5$ and/or $s^*$ decrease: as can be inferred, the relative evaporation rate of the liquid phase with and without crust decreases when the "permeability" (i.e. the ratio $\varepsilon/\tau$) of the crust decreases and when the thickness of the crust increases. For instance, if $P_5$ (i.e. porosity if we assume that the tortuosity is close to one) is lower than 0.1, the instantaneous evaporation rate can be 10 times higher than if there was no crust for very small values of $s^*$.

Consider now the total time of drying through relation (34). The worst cases which can be encountered are obviously the ones for which gradients of solute concentration are extremely strong at the onset of precipitation. Consider the limit case for which the gradient is so strong that the crust thickness tends toward zero (i.e. $s_0^* \approx 1$); from relation (34) one has

$$\frac{t_{\text{drying}}^{\text{crust}}}{t_{\text{drying}}^{\text{no crust}}} = \frac{2}{3} + \frac{1}{3} P_5^{-1} \tag{35}$$

Then, assuming a very low crust porosity of about 0.1, from relation (35) we obtain that the drying time of the remaining water (and therefore the time of concomitant precipitation) would be four times longer than the drying time obtained if there was no crust. The influence of the crust on the evaporation time is significant and this point must be considered when designing SP equipment. Yet a filled particle can finally be obtained provided the volume fraction of the precipitate is sufficient to create a coherent porous medium.

As another example of numerical application, consider again the modelling study of Jayanthi et al. (1993). In the most favourable case, the gas temperature is set to 90 °C and when the solute concentration at the droplet surface reaches the critical supersaturation $c_{\text{ZHC}}^{\text{css}}$, the solute concentration at the droplet centre is exactly equal to the saturation value (6 mol/l) (see Fig. 2 in Jayanthi et al., 1993): therefore, volume precipitation occurs. The theoretical volume fraction of the precipitate formed at the particle centre is equal to 0.33 (Jayanthi et al., 1993): it is much greater than the critical fraction of 0.16, and thus a solid particle should form.

In the most unfavourable case, the gas temperature is set to 150 °C. When the solute concentration at the droplet surface reaches critical supersaturation, the solute concentration at the droplet centre is equal to 4 mol/l, and therefore precipitation occurs from the surface to a position $r_{\text{int},0}/R_{\text{p}}$ equal to 0.72 (where the solute concentration is equal to the saturation value, see Fig. 2 in Jayanthi et al., 1993). Knowing the following parameters: $c_{\text{ZHC}}^{\text{css}} = 8$ mol/l, $M_{\text{ZHC}} = 159$ g/mol and $\rho_{\text{p}} = 2700$ kg/m$^3$, a surface crust porosity of 0.53 can be calculated. Thus, from relation (34), we can estimate that the evaporation of water in excess (and the concomitant precipitation of the solute) occurs during a period 1.45 times longer than if there was no crust. The theoretical volume fraction of the precipitate formed at the particle centre is equal to 0.23, thus volume precipitation may also occur, unless the interfacial saturation pressure of water in air (which depends on the temperature and on the activity of the solution) reaches atmospheric pressure before evaporation is complete: in this case, the solution boils, gas bubbles may form (Charlesworth & Marshall, 1960; Jayanthi et al., 1993; Reuge et al., 2006) leading to inflation or even rupture of the crust, and hollow or fragmented particles would be obtained. Unfortunately, Jayanthi et al. (1993) did not performed experiments corresponding to their simulations and the morphology of the particles which would be obtained for their operating conditions is unknown.

Finally, it can be concluded that the formation of solute concentration gradients inside droplets during the evaporation stage is not a sufficient criterion to explain the formation of hollow particles. Actually, we think that one of the three following conditions must be fulfilled:

- The volume fraction of the precipitate is too low (Jayanthi et al., 1993) toward the particle centre for a coherent porous medium to be able to form.
- Due to the viscoelasticity of some precipitates, an impermeable crust forms which prevents the remaining water from evaporating and escaping (Lin & Gentry, 2003). This case leads inevitably to the next one.
- The temperature of the liquid phase exceeds the boiling point before complete evaporation of the water. In this case, bubble formation may occur, causing inflation or even rupture of the droplet/particle, and hollow or fragmented morphologies would be obtained.

To emphasize this latter point, the results obtained in our previous study on SP of micronic $Y(NO_3)_3$/water droplets (Reuge et al., 2006) are very significant: it was found by modelling that solute concentration gradients appear neither during the evaporation stage nor during the evaporation/precipitation stage. However, hollow $Y_2O_3$ particles are obtained. On the basis on theoretical considerations and experimental data, our study revealed that large amounts of water bound to the yttrium nitrate molecules are still present at the beginning of the thermolysis stage, and above the boiling temperature of the solvent, a partial liquefaction of the hydrated yttrium nitrate occurs with concomitant release of water vapour and $N_2O_5$.

We can assume that the evacuation of vapour water is easier near the particle surface, and therefore a crust of low hydrated yttrium nitrate is formed whereas at the particle centre, yttrium nitrate is more hydrated and maybe liquid. Whereas the dehydration front moves progressively from the surface to the core, an increasing pressure gradient appears between the particle centre and the particle surface. Due to this phenomenon, particle inflation can occur, and yttrium based material, which is rather viscous when it contains water molecules, tends to be moved from the particle centre towards the surface. The direct consequence is the formation of hollow swollen particles, which can be broken if the permeability of the crust is too low and/or the gas pressure inside the particles too high.

Thus, hollow particles can be obtained by SP during the thermolysis stage without formation of solute concentration gradient during the evaporation stage.

## 4. Conclusion

In order to get a better mastery of the spray pyrolysis process and in particular to determine the main limiting steps of the evaporation stage, a general dimensionless study was performed.

We have shown that this stage can be wholly determined by three dimensionless numbers depending on the operation parameters.

More precisely, relations were established to express the total heat flux required for complete evaporation of the spray as a function of dimensionless numbers and to estimate the total evaporation time directly as a function of operating parameters.

For operating conditions corresponding to industrial requirements (i.e. micronic droplet radii, relatively dense sprays, moderate heating rate leading to evaporation times of a few tens of seconds), it has been shown that the difference between water vapour partial pressures in air and at the droplet surface is small and that gas and liquid temperatures are always equal since the limiting step of the evaporation process is thermal transfer from the reactor walls to the gas and not heat or mass transfer at the droplet surface. For these conditions, phenomena can be described by a very simplified set of equations.

Always for these classical conditions, solute concentration and temperature gradients cannot exist inside droplets. In fact, concentration gradients inside droplets are promoted by rapid heating, large initial droplet radii and low dense sprays.

The wide validity of the equations proposed and of the trends deduced was demonstrated by modelling data from the literature over a wide range of operating conditions. These comparisons allowed subtle interpretations of results obtained by the various authors.

Finally, phenomena occurring during the precipitation stage were analysed to account for the origins of the different particle morphologies. If surface precipitation occurs, a crust is formed. But then, water continues to evaporate, diffusing through the crust with concomitant precipitation progressing towards the particle centre possibly forming a filled particle. Considering a quite unfavourable case in terms of crust porosity, our dimensionless model revealed that the total time of drying was four times longer than if there was no crust. This is significant and must be considered when designing SP equipment.

The formation of strong solute concentration gradients during the evaporation stage does not necessarily result in the production of hollow particles but certainly promotes it.


## Acknowledgements

We gratefully acknowledge J.P. Couderc, J. Dexpert-Ghys, N. Joffin and M. Verelst for valuable discussions. This work was supported by the French Ministère de la Recherche (RNMP/POSUMIC).


## Appendix A

*A.1*

- Dimensional form of equations:

$$v_z \frac{\partial m_d}{\partial z} = -(4\pi R) D_v \rho_a \left( Y_{int} \left( \frac{T_{gas}}{T_{liq}} \right) - Y \right) \tag{A.1}$$

$$(F_w + F_s) Cp_w \frac{\partial T_{liq}}{\partial z} + F_a Cp_a \frac{\partial T_{gas}}{\partial z} - F_s h_{vap} \frac{\partial X}{\partial z} = q(2\pi R_c) \tag{A.2}$$

$$v_z m_d Cp_w \frac{\partial T_{liq}}{\partial z} = \lambda_a R^{-1} (T_{gas} - T_{liq})(4\pi R^2) + v_z h_{vap} \frac{\partial m_d}{\partial z} \tag{A.3}$$

with

$$m_d = \rho_w \tfrac{4}{3} \pi R^3 \tag{A.4}$$

and where $Y_{int}$, the reduced water mass fraction at the droplet/gas interface at the saturation pressure, is defined as

$$Y_{int} = a_w (M_w P_{sat})(M_a P_0)^{-1} \tag{A.5}$$

where $a_w$ is the water activity (actually dependent on $X$ but assumed equal to 1), $M_w$ and $M_a$ the molar weights of water and air, $P_0$ the atmospheric pressure and $P_{sat}$ is the water vapour saturation pressure in air which is given by Reid et al. (1977):

$$P_{sat} = \frac{10^5}{760} \exp \left( 18.3036 - \frac{3816.44}{T_{liq} - 46.13} \right) \tag{A.6}$$

- Derivation of relation (9):

  From the following relation:

$$m_s = \frac{1}{1 + X_0} \rho_w \frac{4}{3} \pi R_0^3 = \frac{1}{1 + X} \rho_w \frac{4}{3} \pi R^3 \tag{A.7}$$

the droplet radius $R$ can be written as

$$R = R_0 \left( \frac{1 + X}{1 + X_0} \right)^{1/3} \tag{A.8}$$

Using (2) and (A.8), the following expression can be obtained:

$$R = R_0 \left( \frac{F_s + F_w - F_a Y}{F_s + F_w - F_a Y_0} \right)^{1/3}$$

and using assumption (*xi*):

$$R = R_0 \left( 1 - \frac{F_a}{F_s + F_w} Y \right)^{1/3}$$

which gives relation (9) in a dimensionless form.

- Adimensionalisation of equations:

Using (9) and (A.4), we have

$$v_z \frac{\partial m_d}{\partial z} = \frac{v_z}{H} \frac{\partial(\rho_w (4/3)\pi R_0^3 (1 - P_1^{-1} Y))}{\partial(z/H)}$$
$$= -\frac{4}{3}\pi t_{evap}^{-1} \rho_w R_0^3 P_1^{-1} \frac{\partial Y}{\partial z^*}$$

and (A.1) becomes (3):

$$\Delta Y = Y_{int}(T^*_{gas}/T^*_{liq}) - Y$$
$$= \rho_w (3\rho_a)^{-1} t_{evap}^{-1} R_0^3 D_v^{-1} R_0^{-1} (1 - P_1^{-1} Y)^{-1/3} P_1^{-1} \frac{\partial Y}{\partial z^*}$$
$$= \rho_w (3\rho_a)^{-1} (t_{evap} R_0^2 D_v^{-1}) P_1^{-2/3} (P_1 - Y)^{-1/3} \frac{\partial Y}{\partial z^*}$$
$$= \rho_w (3\rho_a)^{-1} P_2 P_1^{-2/3} (P_1 - Y)^{-1/3} \frac{\partial Y}{\partial z^*}$$

Similar methods were applied to obtain (4) and (5) from (A.2) and (A.3).

- Derivation of relations (12) and (13):
  From (6) and (8), we can write

$$q^* = 2\pi R_c (t_{evap} v_z) q (F_a C p_a T_0)^{-1}$$

Moreover, we have

$$F_a = \rho_a v_z \pi R_c^2$$

and therefore

$$q^* = 2 t_{evap} q R_c^{-1} (\rho_a C p_a T_0)^{-1} \quad (A.9)$$

which gives relation (12) when $q^* = 10 P_1$.
From (11) and (A.10), one has

$$2 q R_c^{-1} (\rho_a C p_a T_0)^{-1} t_{evap}^2 - 10 P_1 t_{evap} - 9200 R_0^2 D_v^{-1} = 0$$

which is a quadratic equation giving relation (13).

### A.2. Derivation of relation (25)

The solute concentration profile inside the droplet is given by (19). Then, the average solute concentration can be written as

$$\bar{c}_s = \frac{c_s(0)}{(4/3)\pi R^3} \int_{r=0}^{r=R} \exp\left(P_3 \frac{r^2}{R^2}\right) (4\pi r^2)\, dr$$

or

$$\bar{c}_s = \frac{3 c_s(0)}{R^3} \int_{r=0}^{r=R} r^2 \exp\left(P_3 \frac{r^2}{R^2}\right) dr$$

With the help of mathematical software such as Mathematica 5.2, we find

$$\int x^2 \exp(a x^2)\, dx = \frac{x \exp(a x^2)}{2a} - \frac{\sqrt{\pi}\, \mathrm{erfi}(\sqrt{a} x)}{4 a^{3/2}}$$

where $\mathrm{erfi}(x) = -i\,\mathrm{erf}(ix)$.

Therefore, we obtain

$$\bar{c}_s = \frac{3}{2} c_s(0) \left( \frac{e^{P_3}}{P_3} - \frac{\sqrt{\pi}}{2 P_3^{3/2}} \mathrm{erfi}(\sqrt{P_3}) \right)$$

Since the droplet radius is given by

$$R = R_0 \left( \frac{c_{s,0}}{\bar{c}_s} \right)^{1/3}$$

And since the onset of precipitation is reached when

$$c_s(R) = c_{s,0}(0)\, e^{P_3} = c_s^{css}$$

The following expression of the droplet radius at the onset of precipitation is obtained:

$$R_p = R_0 \left[ c_{s,0} \left( \frac{3}{2} c_s^{css} \left( P_3^{-1} - \frac{\sqrt{\pi}}{2 P_3^{3/2}} \frac{\mathrm{erfi}(\sqrt{P_3})}{e^{P_3}} \right) \right)^{-1} \right]^{1/3} \quad (A.10)$$

Thus, from (16) and (A.10), relation (25) is deduced.

### A.3. Derivation of equation (31)

The mass of the liquid phase in the droplet is given by

$$m_{liq} = \tilde{\rho}_{liq} \tfrac{4}{3} \pi r_{int}^3$$

Therefore, we have

$$\frac{dm_d}{dt} = \frac{dm_{liq}}{dt} = \frac{d}{dt}\left( \tilde{\rho}_{liq} \frac{4}{3} \pi r_{int}^3 \right)$$
$$= \frac{4}{3}\pi \left[ r_{int}^3 \frac{d\tilde{\rho}_{liq}}{dt} + \tilde{\rho}_{liq} \frac{d(r_{int}^3)}{dt} \right]$$

It can be easily shown by numerical applications that the first term in brackets of the previous expression is insignificant with regards to the second one, therefore we can write

$$\frac{dm_d}{dt} = \frac{4}{3}\pi \tilde{\rho}_{liq} \frac{d(r_{int}^3)}{dt} = 2\pi \tilde{\rho}_{liq} r_{int} \frac{d(r_{int}^2)}{dt}$$

Thus, taking $R = R_p$, $D_v^p$ instead of $D_v$, and the latter expression, Eq. (A.1) becomes Eq. (31).

## References


Charlesworth, D. H., & Marshall, W. R., Jr. (1960). Evaporation from drops containing dissolved solids. *Journal of AIChE*, *6*, 9–23.

FlexPDE 5 (2006). http://www.pdesolutions.com.

Gardner, G. C. (1964). Asymptotic concentration distribution of an involatile solute in an evaporating Drop. *International Journal of Heat and Mass Transfer*, *8*, 667–668.

Gurav, A., Kodas, T., Pluym, T., & Xiong, Y. (1993). Aerosol processing of materials. *Aerosol Science and Technology*, *19*, 411–452.

Hilfer, R. (1996). Transport and relaxation phenomena in porous media. *Advances in Chemical Physics*, *92*, 299.

Hinds, W. C. (1982). *Aerosol technology*. New York: John Wiley & Sons.

Jayanthi, G. V., Zhang, S. C., & Messing, G. L. (1993). Modeling of solid particle formation during solution aerosol thermolysis—The evaporation stage. *Aerosol Science and Technology*, *19*, 478–490.

Joffin, N. (2004). *Synthèse par pyrolyse d'aérosol et caractérisation de luminophores: $Y_2O_3$:Eu et $Zn_2SiO_4$:Mn pour application dans les panneaux à plasma*. PhD thesis. France: Institut National Polytechnique Toulouse.

Lengorro, I. W., Hata, T., & Iskandar, F. (2000). An experimental and modelling investigation of particle production by spray pyrolysis using a laminar flow aerosol reactor. *Journal of Materials Research*, *15*(3), 733–743.

Lin, J.-C., & Gentry, J. W. (2003). Spray drying drop morphology: Experimental study. *Aerosol Science and Technology*, *37*, 15–32.

Lyons, S. W., Ortega, J., Wang, L. M., & Kodas, T. T. (1992). Multicomponent ceramic powder generation by spray pyrolysis. *Materials Research Society Symposia Proceedings*, *271*, 907–917.

Messing, G. L., Zhang, S.-C., & Jayanthi, G. V. (1993). Ceramic powder synthesis by spray pyrolysis. *Journal of the American Ceramic Society*, *76*(11), 2707–2726.

Nesic, S., & Vodnik, J. (1991). Kinetics of droplet evaporation. *Chemical Engineering Science*, *46*, 527–537.

Pratsinis, S. E., & Vemury, S. (1996). Particle formation in gases. *Powder Technology*, *88*, 267–273.

Ranz, W. E., & Marshall, W. R., Jr. (1952). Evaporation from drops: Part I and Part II. *Chemical Engineering Progress*, *48*(141–146), 173–180.

Reid, R. C., Prausnitz, J. M., & Sherwood, T. K. (1977). *The properties of gases and liquid* (3rd ed.). New York: McGraw-Hill.

Reuge, N., Joffin, N., Dexpert-Ghys, J., Verelst, M., Dexpert, H., & Caussat, B. (2006) $Y_2O_3$ micronic particles synthesised by spray pyrolysis: process modelling and considerations about the particle hollowness. *Journal of Materials Processing Technology*, submitted for publication.

Sano, Y., & Keey, R. B. (1982). The drying of a spherical particle containing colloidal material into a hollow sphere. *Chemical Engineering Science*, *37*(6), 881–889.

Schlünder, E. U. (1964). Temperature und Masseänderung verdunstander Tropfen aus reinen Flüssigkeiten und wässrigen Salzlosungen. *International Journal of Heat and Mass Transfer*, *7*, 49–73.

Shabde, V. S., Emets, S. V., Mann, U., Hoo, K. A., Carlson, N. N., & Gladysz, G. M. (2005). Modeling a hollow micro-particle production process. *Computers Chemical Engineering*, *29*, 2420–2428.

Xiong, Y., & Kodas, T. T. (1993). Droplet evaporation and solute precipitation during spray pyrolysis. *Journal of Aerosol Science*, *24*(7), 893–908.

Yu, H.-F. (1995). Simulation of spray pyrolysis for ceramic powder preparation. *Particulate Science and Technology*, *13*, 149–167.

Yu, H.-F., & Liao, W.-H. (1998). Evaporation of solution droplets in spray pyrolysis. *International Journal of Heat and Mass Transfer*, *41*, 993–1001.

Zallen, R. (1983). *The physics of amorphous solids*. New York: Wiley–Interscience.